Journal of Computational Neuroscience 3, 313–336 (1996)

The Intrinsic Electrophysiological Characteristics of Fly Lobula Plate Tangential Cells: I. Passive Membrane Properties

ALEXANDER BORST AND JUERGEN HAAG
Friedrich-Miescher-Laboratorium der Max-Planck-Gesellschaft, Spemannstrasse 37-39, D-72076 Tuebingen, Germany
borst@sunwan.mpik-tueb.mpg.de

Received February 2, 1996; Revised June 10, 1996

Action Editor: John P. Miller

Abstract. The passive membrane properties of the tangential cells in the fly lobula plate (CH, HS, and VS cells, Fig. 1) were determined by combining compartmental modeling and current injection experiments. As a prerequisite, we built a digital base of the cells by 3D-reconstructing individual tangential cells from cobalt-stained material including both CH cells (VCH and DCH cells), all three HS cells (HSN, HSE, and HSS cells) and most members of the VS cell family (Figs. 2, 3). In a first series of experiments, hyperpolarizing and depolarizing currents were injected to determine steady-state I-V curves (Fig. 4). At potentials more negative than resting, a linear relationship holds, whereas at potentials more positive than resting, an outward rectification is observed. Therefore, in all subsequent experiments, when a sinusoidal current of variable frequency was injected, a negative DC current was superimposed to keep the neurons in a hyperpolarized state. The resulting amplitude and phase spectra revealed an average steady-state input resistance of 4 to 5 MΩ and a cut-off frequency between 40 and 80 Hz (Fig. 5). To determine the passive membrane parameters R_m (specific membrane resistance), R_i (specific internal resistivity), and C_m (specific membrane capacitance), the experiments were repeated in computer simulations on compartmental models of the cells (Fig. 6). Good fits between experimental and simulation data were obtained for the following values: $R_m = 2.5$ kΩcm^2, $R_i = 60$ Ωcm, and $C_m = 1.5$ μF/cm^2 for CH cells; $R_m = 2.0$ kΩcm^2, $R_i = 40$ Ωcm, and $C_m = 0.9$ μF/cm^2 for HS cells; $R_m = 2.0$ kΩcm^2, $R_i = 40$ Ωcm, and $C_m = 0.8$ μF/cm^2 for VS cells. An error analysis of the fitting procedure revealed an area of confidence in the R_m-R_i plane within which the R_m-R_i value pairs are still compatible with the experimental data given the statistical fluctuations inherent in the experiments (Figs. 7, 8). We also investigated whether there exist characteristic differences between different members of the same cell class and how much the exact placement of the electrode (within ±100 μm along the axon) influences the result of the simulation (Fig. 9). The membrane parameters were further examined by injection of a hyperpolarizing current pulse (Fig. 10). The resulting compartmental models (Fig. 11) based on the passive membrane parameters determined in this way form the basis of forthcoming studies on dendritic integration and signal propagation in the fly tangential cells (Haag et al., 1997; Haag and Borst, 1997).

Keywords: dendritic integration, three-dimensional reconstruction, compartmental model, membrane parameters, data base

1. Introduction

One of the most interesting problems in neuroscience concerns the computational capabilities of single nerve cells. Are single nerve cells simple functional units, in analogy to transistors, or is each individual neuron a more sophisticated computational device, the characteristics of which are based on the many detailed

properties of all the various ion channels and subcellular machinery? An answer to this question clearly requires experimental techniques to be accompanied by quantitative theoretical approaches.

In this series of papers, we study the tangential cells of the fly lobula plate. The tangential cells are located in the posterior part of the third visual neuropile of the fly called the *lobula plate* (Fig. 1). With their large dendrites they spatially pool the signals of thousands of local, motion-sensitive elements arranged in a columnar fashion. The tangential cells thus have large receptive fields and respond to visual motion in a directionally selective way (Borst and Egelhaaf, 1989, 1990). They either connect to other brain areas or, via descending neurons, to thoracic motor centers. From various lines of evidence it is concluded that the tangential cells are involved in the fly's visual course control (Geiger and Nässel, 1981, 1982; Hausen and Wehrhahn, 1983, 1990; Heisenberg et al., 1978; Borst and Bahde, 1988; Borst, 1990, 1991).

These neurons serve as a model system to study dendritic processing and signal propagation within single nerve cells (Haag et al., 1992; Borst et al., 1995; Borst and Egelhaaf, 1994) because of several advantageous features: (1) The tangential cells represent a set of about 60 fairly large neurons per brain hemisphere and each cell can be identified due to its invariant anatomy and characteristic visual response properties (Hausen, 1981, 1982a, 1982b, 1984; Hengstenberg, 1982; Eckert and Dvorak, 1983). This allows the repetition of measurements on the same cell in different animals. (2) The cells are amenable to various electrophysiological, pharmacological and optical recording methods *in vivo* (Borst and Egelhaaf, 1992; Egelhaaf and Borst, 1993, 1995) and *in vitro* (Brotz et al., 1995). (3) The cells can be visually stimulated, thereby driving their input synapses with the same input as under natural conditions. The retinotopic input organization of the cells furthermore allows the stimulation of selected dendritic branches with either excitatory or inhibitory input (Borst and Egelhaaf, 1992; Haag et al., 1992; Egelhaaf et al., 1993, 1994).

In the following sections, we first describe the construction of a digital data base that relates, through compartmental modeling, the anatomy of the cells to their computational properties. To determine the passive membrane parameters of the cells, current injection experiments were performed in a voltage regime where the current-voltage relationship in the neurons was linear. The data were compared with the responses of the compartmental model cells in computer simulations. By varying the passive membrane parameters of the model cells in a systematic way, the appropriate set of membrane parameters was determined.

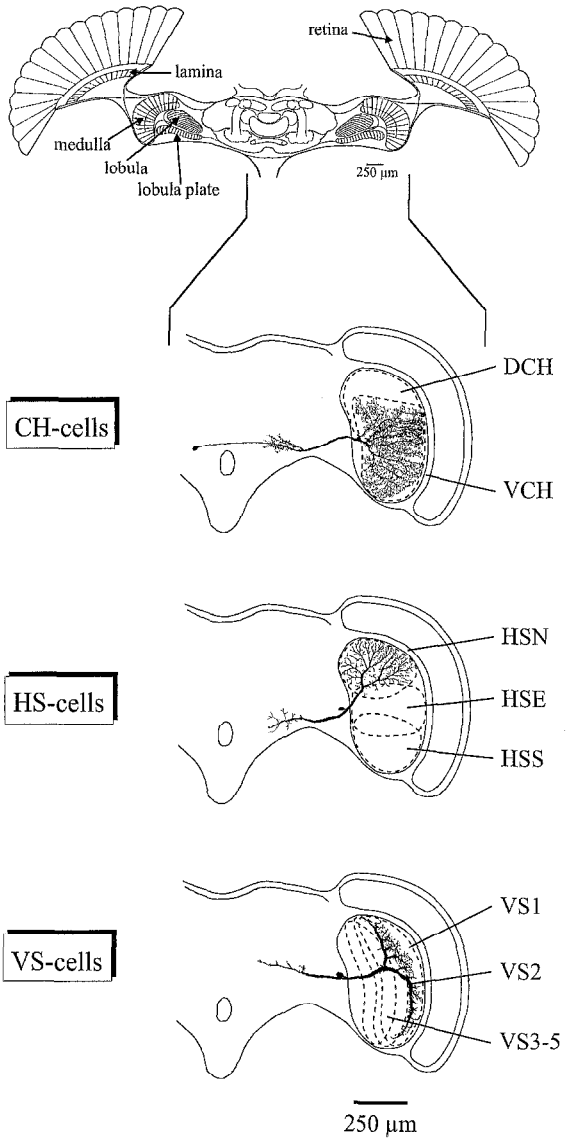

Figure 1. Schematic horizontal cross-section through the head of a fly including the major parts of its head ganglion (top). Below, one representative of each of the three cell families of the lobula plate tangential cells considered in this article are shown in a frontal view (CH, HS, and VS cells, from top to bottom). The dendritic fields of other members of each cell family are also indicated by dashed lines. Note that within each cell family, all members fill the space of the lobula plate by occupying different but overlapping areas with their large dendrites. Per brain hemisphere, there exist two different CH cells (a *d*orsal DCH and a *v*entral VCH cell), three different HS cells (a *n*orthern HSN, an *e*quatorial HSE, and a *s*outhern HSS cell), and eleven different VS cells (numbered from the lateral VS1 to the most proximal VS11 consecutively).

These results will form the basis for studies on voltage-activated membrane currents and visual response properties of the fly lobula plate tangential cells (Haag et al., 1997; Haag and Borst, 1997) with the aim of understanding in detail the biophysical basis of dendritic processing and signal propagation in single nerve cells.

2. Material and Methods

2.1. *Preparation and Set-up*

Female blowflies (*Calliphora erythrocephala*) were briefly anesthesized with CO_2 and mounted ventral side up with wax on a small preparation platform. The head capsula was opened from behind; the trachea and air-sacs, which normally cover the lobula plate, were removed. To eliminate movements of the brain caused by peristaltic contractions of the oesophagus, the proboscis of the animal was cut away and the gut was removed from the head capsule. This allowed stable intracellular recordings of up to 45 minutes. The fly was mounted in an upright position on a heavy recording table with the stimulus monitors in front of the animal. The fly brain was viewed from behind through a Zeiss dissection scope.

2.2. *Recording*

Electrodes were pulled on a Brown-Flaming micropipette puller (P-77) using thin-wall glass capillaries with a diameter of 1 mm (Clark, GC100TF-10). When filled with 1*M* KCl they had resistances of about 20 to 30 MOhm. We used an SEC-10L amplifier (npi-electronics) throughout the experiments usually operated in the switched-electrode current clamp mode at a switching frequency of 20 kHz. For cobalt injection, electrodes were filled with 7% Cobalt hexamine chloride resulting in an average resistance of about 80 MΩ and the amplifier was operated in the bridge mode. To fill the cells, we applied a depolarizing current of up to 5 nA for 5 to 15 minutes. For data analysis, the output signals of the amplifier were fed to an IBM PS/2 via a 12 bit A/D converter (Data Translation DT2801-A) at a sampling rate of 20 kHz. The programs for the evaluation of the data were written in Turbo-Pascal (Borland).

2.3. *Stimulation*

To identify the cells during the experiment by their visual response properties, two monitors (Tectronix 608) were placed in front of the animal. They were positioned at an angle of + and −45° from the fly's frontal midline. The position of the animals was carefully adjusted using the symmetry of the frontal equatorial pseudopupils of both eyes (Franceschini and Kirschfeld, 1971). As seen by the fly, the displays had a horizontal angular extent of 68° and a vertical extent of 81°. The stimulus pattern was produced by an image synthesizer (Picasso, Innisfree Inc.) that was controlled by an IBM PS/2. The intensity of the pattern was square-wave modulated along its horizontal axis. The stimulus grating had a fixed wavelength of 14° and a contrast of 0.70. The mean luminance of the pattern was about 25 cd/m^2. Before current injection was started, cells were stimulated by the pattern moving back and forth with a duty cycle of 2 s. Cells were identified by their preferred direction of visual motion stimuli and by the location and extent of their receptive field.

2.4. *Histology*

We used the method of silver intensified cobalt sulphide impregnation (Strausfeld and Hausen, 1977). After filling a cell with cobalt for sufficient time, the electrode was withdrawn, and the cobalt ions were allowed to diffuse for about one hour. Then, the head was completely opened under a dissection microscope and exposed to a solution of ammonium sulphide (five drops in 10 ml distilled water) for 5 minutes. The tissue was washed with ringer and subsequently fixed in 80 ml 100% ethanol, 8 ml acetic acid, and 12 ml formalin (AAF). The head ganglia were transferred to 30% ethyl alcohol. They were washed and then incubated in gum arabic (10 vol) with 1% hydroquinone (1 vol) and 10% citric acid (2 vol) for 20 mins at 50°C. Then, the tissue was incubated at 50°C in the dark for about 1 to 2 hours in a solution containing gum arabic (10 vol), 10% hydroquinone (1 vol), and 10% citric acid (1 vol), plus 1% silver nitrate (1 vol) until a silver-grey precipitate became visible at the surface of the tissue. The tissue was then transferred to 1% acetic acid solution in 30% ethyl alcohol for 10 mins. After dehydration through graded alcohols, the brain was washed in propylen oxide and embedded in Araldite (polymerized in an oven at 60°C) on slides for visual inspection. To investigate tissue shrinkage due to the histological procedure, we measured the brains of 5 flies before (that is, in vivo) and after the end of the procedure (when embedded in Araldite). On average, the size was found to be reduced by about 16% along the transversal axis (measured between the distal rims

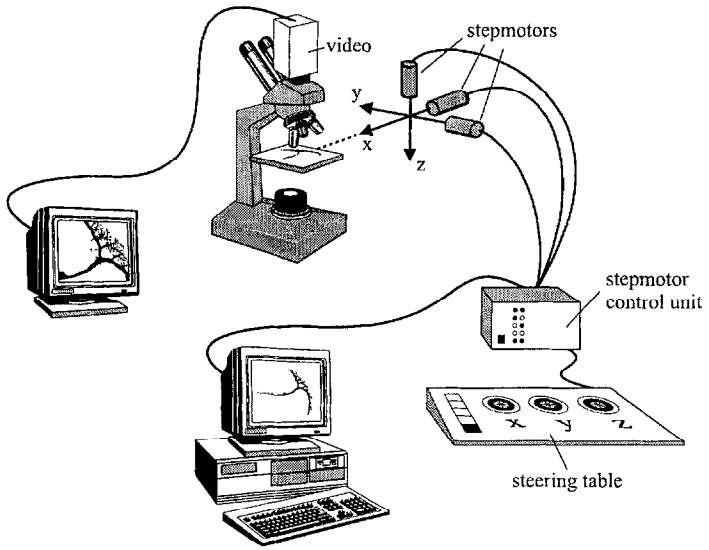

Figure 2. Outline of the reconstruction set-up used for digitizing the anatomy of the cells. The preparation is viewed through a microscope equipped with a video camera that is connected to a monitor. The microscope stage is movable in all three spatial axes by means of three step motors. The step motors are controlled by dials and, in addition, by a computer. The computer also reads continuously the positions of the step motors.

of the left and right medulla) and by about 18% along the dorsoventral axis of the brain.

2.5. *3D Reconstruction*

See Fig. 2. The fly brain with the cobalt-stained neuron was mounted as a whole mount under an upright microscope (Zeiss Standard) using a 63× Neofluar oil immersion lens with 1.25 NA and a long working distance. A video camera on the camera port of the microscope was connected to a video monitor. The preparation was moved in all three axes by three orthogonally mounted step motors (Mini 25, Luigs and Neumann) connected to an electronic control device. This unit was connected to a computer (286 PC) and to a panel equipped with three dials for manual control. The step motors act with a precision of below 1 μm and are drift free. The position of all three motors was continuously read out by the computer via the serial port (RS232). The preparation could be moved either manually by the handwheels or by a command from the computer through the serial port. The software (written in Turbo Pascal, Borland) was developed in our laboratory using a commercial unit (from Luigs and Neumann) for communication with the step motor control unit. The procedure for reconstruction of a neuron was as follows. After bringing a certain point of the neuron in focus and centering it, the reconstruction software is invoked on the PC. When started, the program read in the current step-motor positions as the zero point of its coordinate system. Using the dials, the preparation was then shifted for a few μm along one branch. The x-, y-, and z-coordinates were contineously displayed on the computer screen. On key stroke, the coordinates became entered into an ASCII file. Two more pieces of information on this entry point are needed: the diameter of the branch, which was measured from the video monitor using a hand-held ruler, and the identification letter, which was either a *C* (*c*ontinuation, two neighbors), a *B* (*b*ranch point, three neighbors), or a *T* (*t*erminal, one neighbor). Then a line was drawn on the computer screen between the previous and the actual digitized point. The preparation could now be moved to the next point being digitized and so on.

Since the branched structure of a neuron requires some logic of the links between several points within the sequential file, the nested hierarchy has to be taken care of. This implies that after a terminal point, the next point in the file is attached to the last open branch point. Obviously, a branch is complete after it is followed by two terminal points. The digitizing software supports this logic by moving automatically to the last open branch point after a terminal point has been entered.

In order to test how reliable our reconstruction system operates, we had one and the same cell digitized twice by two different persons. The cell was a VS4 cell, and the reconstructions yielded similar results. Both reconstructions are shown in stick figure mode

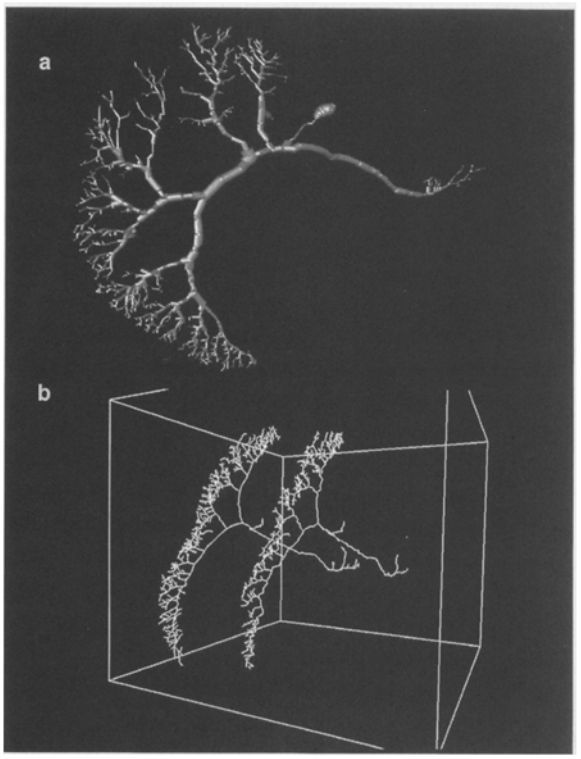

Figure 3. (a) Example of a digitized fly tangential cell (VS1) as viewed after 3D reconstruction. The cell is not shown plane-parallel but rotated by 20 to 30° around the dorso-ventral axis with the dendrites toward the viewer. (b) An identical tangential cell (VS4) digitized twice by two different operators. Cells are displayed in the stick figure mode.

in Fig. 3(b). The only obvious difference pertains to the ventral-most tips of the dendrite where some small branches have been missed in one reconstruction. The number of compartments amounts to 1,004 (cell 1) and 988 (cell 2), respectively. Measured from the main branch point where the axon originates from the dendrite, the distance to the axon terminal is 637 μm (cell 1) and 633 μm (cell 2), the distance to the dorsal tip of the dendrite is 266 μm (cell 1) and 280 μm (cell 2), and the distance to the ventral tip of the dendrite is 412 μm (cell 1) and 405 μm (cell 2). We thus conclude that the error introduced by our reconstruction set-up in combination with the variability of the human operator is well below 5% of the anatomical values indicated.

2.6. *Display Software*

For a display of the shape of the neuron incorporating information about diameters, we extended software originally written by Frederic Theunissen, University of California at Berkeley, that runs under UNIX on any workstation supporting GL graphics language. The software reads the ASCII file created by the digitizing software and displays the neuron initially in a stick figure. In this mode, the user can rotate the cell around all three axes in real time, zoom in and out, and draw or remove a wire cube and a central coordinate axes system on the screen. If a particular viewing angle seems satisfying to the user, the cell can be displayed in 3D solid shape on key stroke. The cell is then displayed as a series of tubes connecting all the digitized points using the nested hierarchy logic with the diameter of the tubes equaling the diameter of the neuron at this point (Fig. 3(a)). Since the neurons typically had several thousands of vectors, the reconstruction of such a solid object required up to 30 s. We find the optional switch between the fast but rudimentary stick-figure mode and the realistic but computationally demanding tube mode most useful to rapidly aquire a faithful three-dimensional representation of the nerve cell in the observer's mind. The display software also allows a three-dimensional view of the cell using stereo glasses with liquid crystal shutters synchronized with the monitor.

2.7. *Computer Simulations*

For compartmental model simulations we used the software package Nemosys developed by Frederic Theunissen et al. (Theunissen et al., 1996; Eeckman et al., 1994) in John Miller's laboratory. Nemosys reads the ASCII file, which contains the anatomical data of a single cell. For each user-defined part of the cell, all individual active and passive membrane parameters can be manually set and manipulated. Among many other features, Nemosys allows the placement of many simulated electrodes for current injection and recording throughout the cell. These electrodes can be operated in the current or voltage clamp mode. The resulting membrane potential changes are displayed as an animated sequence, with the cell's membrane potential coded in false color, plus the electrode signals displayed conventionally as a function of time. All membrane parameters can also be controlled through ASCII files. Using this feature, we varied the passive membrane resistance, internal resistivity, and membrane capacitance in a systematic way. Calculating the amplitude and phase spectra with this given set of parameters and minimizing the error between the simulated and experimental

data allowed us to search for the set of parameters that gave us the optimal fit. Since the parameter search is not a feature of Nemosys, we used the Origin Software (Microcal Software Inc., Northampton, MA, USA) with the LabTalk macro language for this purpose, operating on the ASCII file output produced by Nemosys.

3. Results

3.1. Digital Data Base

So far we have digitized a total of 15 tangential cells of the fly lobula plate. Our data base currently comprises six members of the HS cell family, seven members of VS cells, and two CH cells. Some of these cells are shown in Fig. 1 in a frontal projection within the outlines of the neuropile where they arborize. As has been described earlier (Hausen, 1981, 1982a, 1984; Eckert and Dvorak, 1983; Hengstenberg et al., 1982; Hengstenberg, 1982), the dendritic arbors of the different members within one family occupy different but overlapping areas in the lobula plate in such a way that each family completely covers the lobula plate. An example of lobula plate VS1-cell is shown in 3D solid shape in Fig. 3(a) using our display software. Reconstructions of several representatives of the same cell obtained from stainings in different flies reveal a high degree of anatomical constancy (not shown). This constancy not only pertains to the area of dendritic arborization in the lobula plate, the track of the axon, and the region of the axon terminal but also to the major dendritic branches including the general branching topology. A complete set of all tangential cells digitized in our laboratory can be inspected through the World Wide Web at the Flylab home page with the following address: http://wwwfml.mpib-tuebingen.mpg.dc/borst/.

Comparing different cell families one immediately sees that these cells have a different overall topology. Although the exact location along the longitudinal body axis can only be estimated (no neuropil markers have been taken along this coordinate), the following striking features appear in the 3D representation of the cells: (1) At the distal edge of the lobula plate, HS and CH cells bend their dendritic tips toward the anterior of the brain. This is due to the curvature of the otherwise flat lobula plate in this region. (2) The dorsal dendritic branches of VS1 cells seem to occupy different, more anterior layers of the lobula plate than do the rest of their dendrite. This feature has been noticed before (Eckert, 1982; Hengstenberg et al., 1982) but becomes easily evident when rotating a VS1-cell in 3D space and looking at it under various viewing angles.

3.2. I-V Relationships

In a first series of experiments, the cells were impaled with a sharp electrode in their axon at or close to the place where the axon crosses the border between the lobula plate and the central brain area. The cells had resting potentials between −40 and −55 mV. Operating the amplifier in the switched electrode current clamp mode, depolarizing and hyperpolarizing current pulses of 100 ms duration and variable magnitude were injected into the cells. The resulting membrane potential deviation from resting is shown in Fig. 4, left panel, for each of the cell types (CH, HS, and VS cells, from top to bottom). All three cell types responded to hyperpolarizing currents in a way which was expected for a linear low-pass filter with a short time-constant of well below 10 ms. As can be seen from the potential traces in Fig. 4, no obvious nonlinearity like anomalous inward rectification was detectable in this voltage range. In contrast, in response to depolarizing current pulses, all cell types exhibited pronounced nonlinearities: When the amplitude of the current exceeded a certain threshold value, CH cells showed an initial hump, and HS and VS cells responded with strong transient spike activity. Moreover, the plateau response to depolarizing current pulses was strongly reduced as compared to hyperpolarizing current pulses of the same amplitude.

To evaluate the current-voltage relationship quantitatively and in a statistically significant way, experiments like the one shown on the left side of Fig. 4 were done for many neurons of all three-cell families. For each cell and for each amplitude of current injection, the experiment was repeated 10 times. The resulting membrane potential deviation from resting was determined 70 ms after the beginning of the current injection for each sweep and averaged over all 10 sweeps. In this way, the current-voltage relationship was determined in 16 different CH cells (comprising recordings from DCH and VCH cells), 28 different HS cells (comprising recordings from HSN and HSE cells), and 9 different VS cells (comprising recordings from VS1 to VS5 cells). The mean data are shown together with the standard error of the mean on the right side of Fig. 4. Clearly, a linear current-voltage relationship holds in the hyperpolarizing range, while a nonlinear outward rectification is observable for depolarizing currents. In

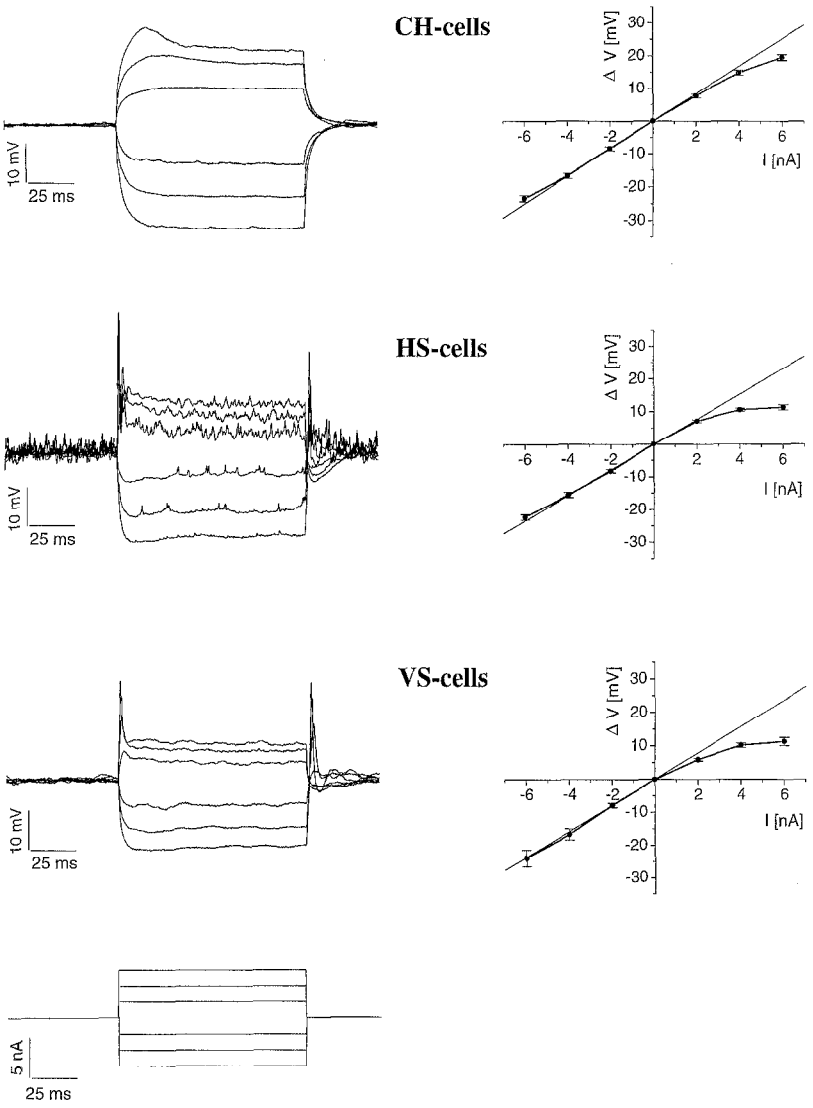

Figure 4. Left panel displays membrane potential of CH, HS, and VS cells (from top to bottom) as a function of time following pulse-like current injection of various amplitudes. The bottom graph shows the time course of the current applied. Note that HS and VS cells respond with an initial spike to depolarizing currents while CH cells do not. Each data trace represents the average of 5 sweeps. The right panel shows I-V curves of CH, HS, and VS cells (from top to bottom) obtained from a 100 ms pulse injection of the current indicated on the x-axis. The resulting voltage change was measured 70 ms after the start of the current injection. As can be seen, the current-voltage relationships are linear below resting potential for all three cell types and show a more or less significant outward rectification above resting potential. Values are the mean ± SEM measured in 16 CH, 28 HS, and 9 VS cells, respectively.

the voltage range more negative than resting, an average input resistance of 4 to 5 MΩ was derived for all cell types.

3.3. *Amplitude and Phase Spectra*

To determine the passive membrane properties of tangential cells, we analyzed the responses of the cells to current injection waveforms that kept the cells in the voltage range where a linear current-voltage relationship held. One way to assess the important passive parameters R_m, R_i, and C_m consists in determining the input resistance as a function of frequency of the injected current. Theoretically, there is a number of ways of doing it (see Discussion for further explanation of this point). We decided to apply each frequency

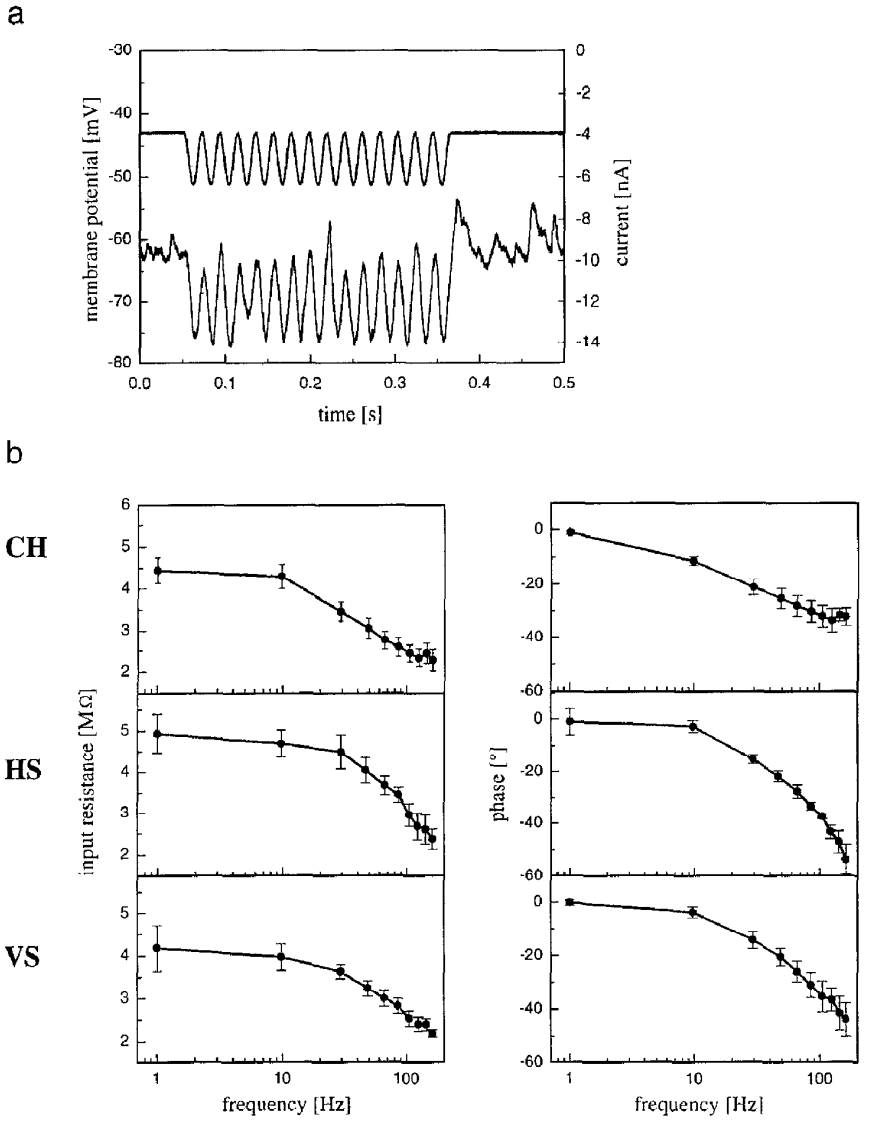

Figure 5. (a) Example of a sinusoidal current injection of 1.2 nA amplitude superimposed on a hyperpolarizing DC current of −5 nA. The upper curve represents the current applied (indicated on the right y-axis); the lower curve represents the membrane potential of the cell (indicated on the left y-axis). Note that the cell (HS cell) follows with its membrane potential the current in an almost sinusoidal way. (b) Amplitude and phase spectra of CH, HS, and VS cells (from top to bottom) obtained from injection of a sinusoidal current of 1.2 nA amplitude and variable frequency (indicated on the x-axis) into the cells while hyperpolarizing them with a DC current of −5 nA. The steady-state input resistances (amplitude value at lowest frequency) ranges from 4 to 5 MΩ. The cutoff-frequency is lowest for CH cells (40 Hz) and higher for HS (80 Hz) and VS cells (78 Hz). Phase spectra show a maximum phase shift of about −60 deg at the highest frequency tested (160 Hz). Values are the mean ⊥ SEM measured in 6 CH, 5 HS, and 5 VS cells, respectively.

separately by injecting a sinusoidally modulated current of 1.2 nA amplitude superimposed on a 5 nA hyperpolarizing DC current.

One such experiment done on an HS cell is shown in Fig. 5(a). The cell's membrane potential followed the current, which was modulated with a frequency of 50 Hz in a more or less sinusoidal way. For a quantitative analysis we repeated such an experiment on all cell types using 10 different frequencies (from 1 to 160 Hz) and 10 sweeps per frequency. Simultaneously, the injected current was read into the computer. The membrane and current signals of all sweeps of one frequency and cell were averaged. These data were then Fourier transformed and their amplitude and phase spectra were

calculated. The amplitude spectrum of the membrane signal was then divided by the amplitude spectrum of the injected current to give the input resistance as a function of frequency. This function is shown for the different cell types (CH, HS, and VS cells, from top to bottom) in the left panels of Fig. 5(b). To the right, the respective phase spectra are shown. Note that all data are presented in semilogarithmic plots. The input resistance of all cell types at the lowest frequency tested—that is, at 1 Hz, is between 4 and 5 MΩ. This value is identical to the steady-state input resistance as determined from the current pulse-injection experiments shown in Fig. 4. At higher frequencies, the input resistance drops markedly, as is expected for a passive resistor-capacitor network. The corner frequencies as defined by a 3 dB reduction of the input resistance is lowest for CH cells (about 40 Hz) and higher for HS and VS cells (about 80 Hz for both cell types). In a similar way, the phase spectrum starts to deviate significantly from 0° at 10 Hz in the CH cells. For HS and VS cells, the deviation begins at 30 Hz. For CH cells, the maximum phase shift observed at 160 Hz resulted in approximately 35°, for HS and VS cells, the maximum phase shift is between 50 and 60°.

3.4. *Fitting Membrane Parameters of Model Cells*

For which membrane parameters can these experiments be fit best by compartmental models of the various cell types? To answer this question, we simulated these experiments using the Nemosys compartmental model software (Theunissen et al., 1996) with our data base as a source. In a first set of simulation studies, we calculated responses in all digitized CH, HS, and VS cells at the location that corresponds to the experimental electrode placement. Assuming spatially homogeneous membrane parameters, we determined the amplitude and phase spectra for 450 different triplets of R_m, R_i, and C_m. The values for R_m were varied from 20 Ωcm^2 to 20 kΩcm^2 in 10 steps (20, 50, 100, 200, ..., 20,000), the values for R_i ranged between 5 Ωcm and 2 kΩcm in 9 steps (5, 10, 20, 50, ..., 2,000), while C_m was altered between 0.5 and 1.5 μF/cm^2 in steps of 0.25. The amplitude and phase spectra obtained for each cell and each parameter constellation then were averaged within each cell family. The resulting average spectra for each cell family subsequently were compared with the corresponding experimental data using the following formulas:

$$E_{A,\mathrm{SIM}} = \sqrt{\sum_{i=1}^{i=10}(A_{\mathrm{exp},i} - A_{\mathrm{sim},i})^2}; \quad (1)$$

$$E_{A,\mathrm{EXP}} = \sqrt{\sum_{i=1}^{i=10}(\sigma_{A,i})^2}; \quad (2)$$

$$E_{\Theta,\mathrm{SIM}} = \sqrt{\sum_{i=1}^{i=10}(\Theta_{\mathrm{exp},i} - \Theta_{\mathrm{sim},i})^2}; \quad (3)$$

$$E_{\Theta,\mathrm{EXP}} = \sqrt{\sum_{i=1}^{i=10}(\sigma_{\Theta,i})^2}; \quad (4)$$

$$E(R_m, R_i, C_m) = 0.5 * (E_{A,\mathrm{SIM}}/E_{A,\mathrm{EXP}} + E_{\Theta,\mathrm{SIM}}/E_{\Theta,\mathrm{EXP}}); \quad (5)$$

In these formulas A and Θ represent the amplitude and phase values for all frequencies tested experimentally. The indices i ranging from 1 to 10 correspond to the following frequency values: 1, 10, 30, 60, 80, 100, 120, 140, 160, and 180 Hz. Equation (1) determines the error function according to the amplitude values as the square root of the sum of the squared differences between the mean experimental amplitudes $A_{\mathrm{exp},i}$ and the simulated values $A_{\mathrm{sim},i}$ for each frequency f_i. Equation (2) determines the error inherent in the experimental data by calculating the square root of the sum of σ squared, with σ being the standard error of the mean obtained from the experimental data. The same procedure is done in Eqs. (3) and (4) for the error in the phase spectra. In Eq. (5) these error values are combined by first dividing the amplitude error $E_{A,\mathrm{SIM}}$ obtained from comparing simulated and experimental data by the error $E_{A,\mathrm{EXP}}$ equivalent to the statistical fluctuations inherent in the experimental data and then doing the same for the phase errors $E_{\Theta,\mathrm{SIM}}$ and $E_{\Theta,\mathrm{EXP}}$. These two ratios are summed with equal weight in Eq. (5). Having determined the spatially homogeneous triplet of R_m, R_i, and C_m values leading to a minimal error in this way, a more fine scale search was done centered around the previously found minimum with the following step widths: $\Delta R_m = 0.5$ kΩcm^2, $\Delta R_i = 20$ Ωcm, and $\Delta C_m = 0.1$ μF/cm^2. This led to the parameter triplets for each cell type summarized in Table 1. The values of the error function for the optimal parameter set are indicated in the rightmost column of Table 1. These values are similar for all cell types. Given this set of passive membrane parameters

Table 1. Passive membrane parameters.

Cell family	R_m ($\Omega \cdot cm^2$)	R_i ($\Omega \cdot cm^2$)	C_m ($\mu F/cm^2$)	Error
CH cells	2.5 k	60	1.5	0.64
HS cells	2.0 k	40	0.9	0.71
VS cells	2.0 k	40	0.8	0.70

the resulting amplitude and phase spectra are shown in Fig. 6. For comparison, the experimental data from Fig. 5(b) are shown as dashed lines in all panels again. As can be seen from comparing experimental and simulated results in Fig. 6, the parameters chosen lead to a rather close fit between both data sets.

3.5. *Ambiguity of Extrema*

Does this indicate that the real fly tangential cells indeed possess the respective membrane parameters that are indicated in the left three panels of Fig. 6? Different scenarios are possible. First, it could be that there are many completely different parameter sets that are more or less in good agreement with the experimental results. This would mean that the respective error function has several local minima. Another possibility is that given the experimental error inherent in the electrophysiological data due to unavoidable statistical fluctuations and the error due to imprecision in the reconstruction of the cells, the volume in the R_m-R_i-C_m space within which the simulated data lead to a fit with the experimental data is so large that again no solid statement on the precise values of R_m, R_i, and C_m can be made on the basis of existing experimental data.

To answer these questions, a close inspection of the respective error functions was necessary. The error functions used to yield the optimal fit in Fig. 6 are shown in the left column of Fig. 7 as 3D plots for all three different cell types (CH, HS, and VS cells, from top to bottom). Here, the third parameter C_m is constant and equal to 1.5 $\mu F/cm^2$ (CH cells) or 1.0 $\mu F/cm^2$ (HS and VS cells), respectively. Note that, for the sake of better visibility, the negative logarithm of the error function is displayed, turning a dip into a peak and

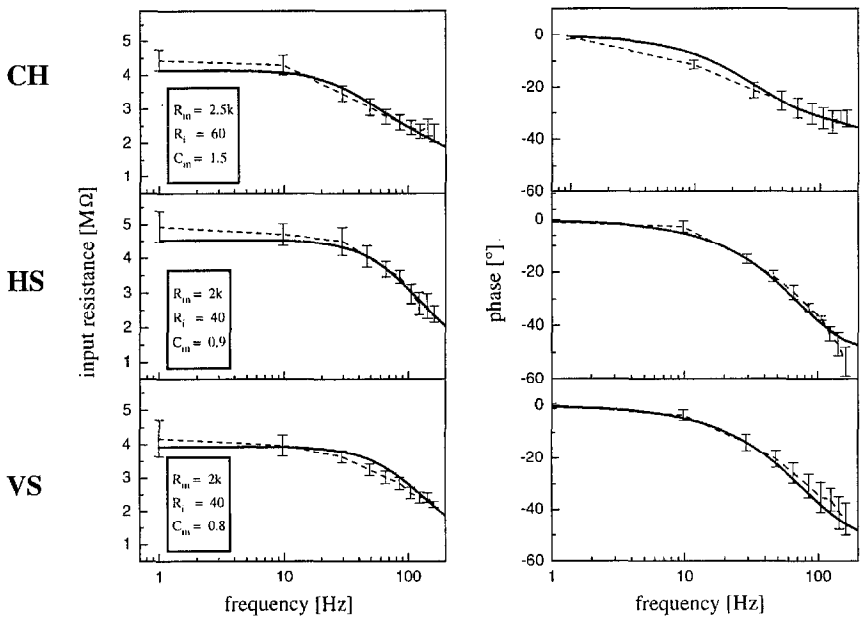

Figure 6. Amplitude and phase spectra of CH, HS, and VS cells (from top to bottom) as obtained from compartmental model simulations taking into account the detailed anatomy of each cell type. The protocol used in the simulations was exactly the same as in the experiments (see legend of Fig. 5). Cells were modeled using the Nemosys software. They had no voltage-dependent conductances. All passive parameters were assumed to be spatially homogeneous. The exact values of the membrane parameters used for the amplitude and phase spectra shown in this figure were determined by minimizing an error function between the experimentally determined curves (dashed lines, values taken from Fig. 5) and the responses of the compartmental model cells of each cell type. The values resulting in a minimum error are indicated within each amplitude spectrum and were the same for the respective phase spectrum (R_m in Ωcm^2, R_i given in Ωcm, and C_m in $\mu F/cm^2$). The simulation data represent the mean responses of 2 CH, 6 HS, and 4 VS cells. Note that all three specific membrane parameters R_m, R_i, and C_m were varied to find the optimum fit.

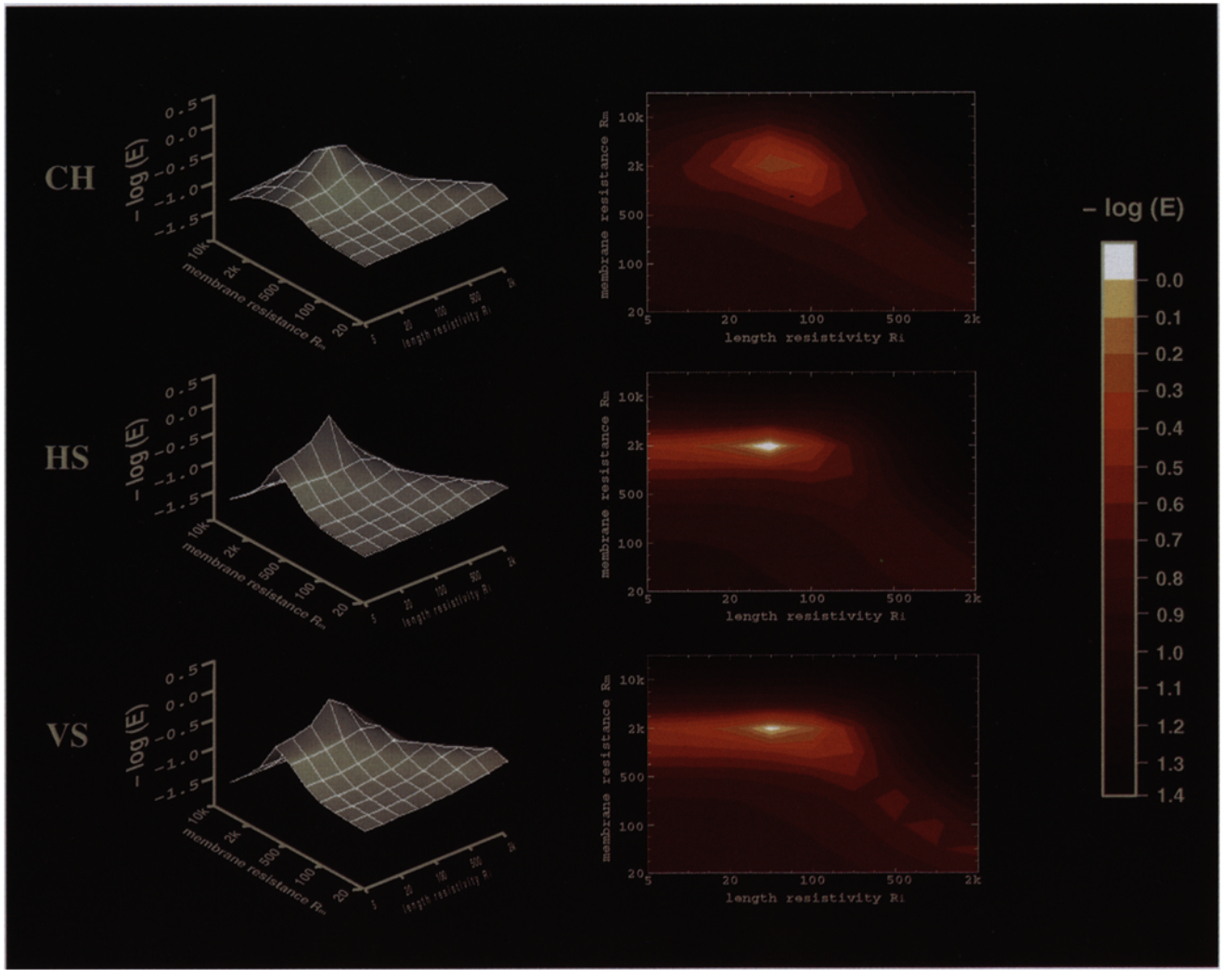

Figure 7. Error functions E in dependence of the specific membrane resistance R_m and the internal resistivity R_i with a value of 1.5 (CH cell) and 1.0 (HS and VS cells) μF/cm^2 for the specific membrane capacitance C_m. The functions are shown for the three different cell types—CH, HS, and VS cells (from top to bottom). Roughly, the error function E is defined as the summed squared differences between the amplitude and phase spectra obtained from compartmental model simulations of the various cell types and the respective experimental values (for exact definition see text). Here, the negative logarithm of E is plotted for the sake of better visibility of the extremum. To the left the functions are shown as 3D plots; to the right contour line plots represent a top view of the error functions in false color code. The white area in the contour plot represents the area of confidence within which the values of R_m and R_i are still compatible with the experimental data given their statistical fluctuations. The color code as shown by the bar to the right indicates $-\log(E)$. Thus, the topmost color (white) codes for a range where E is smaller than 1.

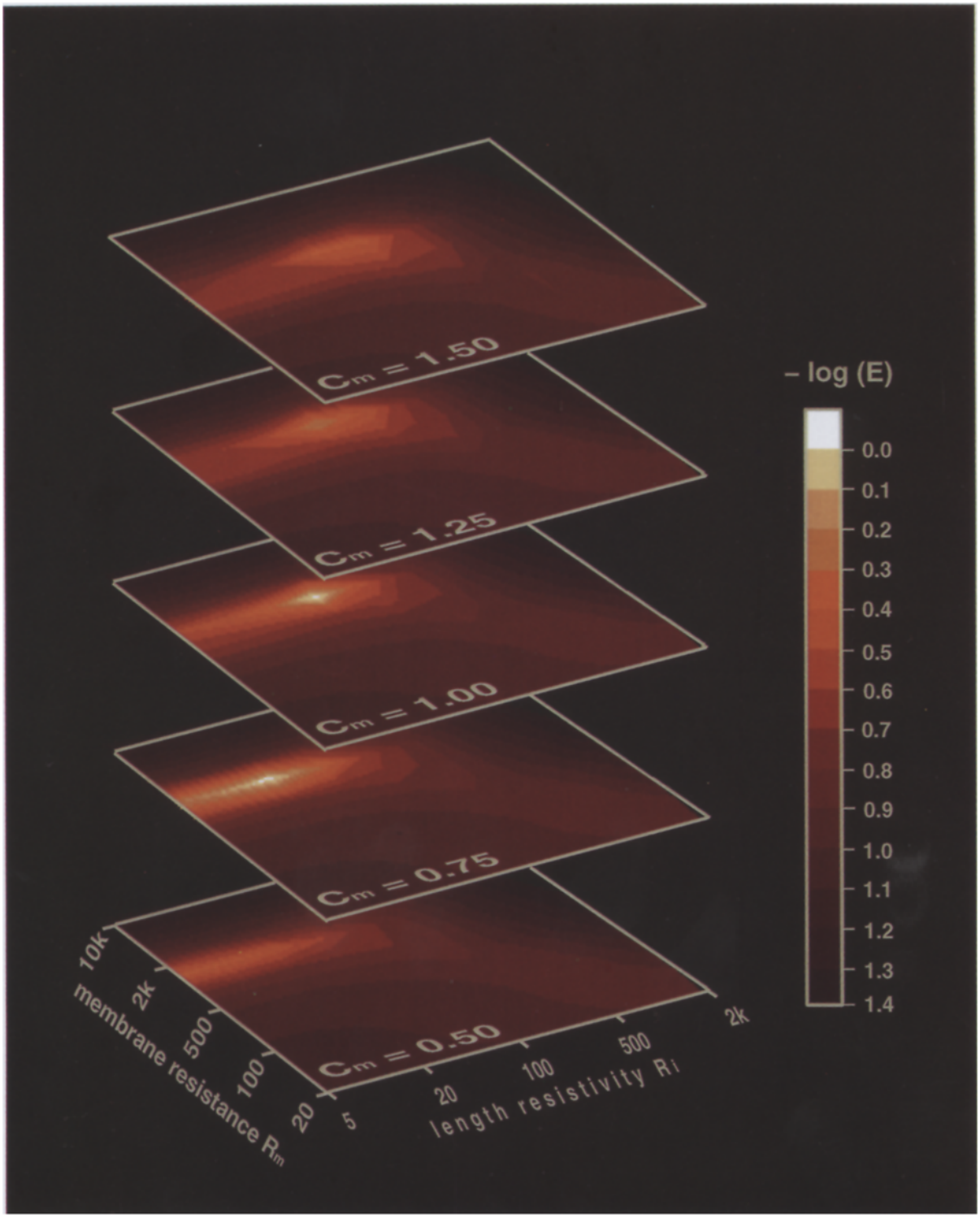

Figure 8. Volume visualization of the error value E as a function of R_m, R_i, and C_m for HS cells. The 3D function is sliced parallel to the R_m-R_i plane at five different C_m values, indicated to the right. This can also be understood as having a stack of contour plots viewed in perspective. As can be seen, the optimum shifts toward smaller values of R_i with decreasing C_m values. However, the maximum of the function—the optimal fit between experimental and simulation data—is obtained at a C_m value between 0.75 and 1.0 μF/cm^2. The color code as shown by the bar to the right indicates $-\log(E)$. Thus, the topmost color (white) codes for a range where E is smaller than 1.

stretching the interesting part of the function around the extremum. In the right column, contour plots of the error functions are displayed. The white area, where $E < 1$, demarks those R_m-R_i pairs for which the error between the simulated function and the mean experimental value is smaller than the standard error of the mean of the experimental data (where the negative logarithm of the ratio, $-\log(E)$, is larger than zero). It thus represents the area of confidence within which the pairs of R_m-R_i values are still compatible with the data, given the statistical fluctuations inherent in the measurements. As it turns out, the error functions reveal a monotonic structure with a single extremum for all three cell types. Thus, the possibility of being trapped in only a local minimum can be excluded. Furthermore, as is revealed by close inspection of the area of confidence, no substantial variation of the resistance values is allowed for by the experimental data.

With the large step width used in this logarithmic scan of the parameter plane, the error function never becomes smaller than 1 for CH cells. The extremum centers around $R_m = 2\,\text{k}\Omega\text{cm}^2$, and $R_i = 60\,\Omega\text{cm}$. For both HS and VS cells, better fits are yielded even given the large parameter step width. In both cell families, the error function becomes smaller than 1 in certain regions of the of R_m-R_i-plane. In HS cells both 50 and 100 Ωcm values of R_i are tolerated, with R_m being fixed at 2 $\text{k}\Omega\text{cm}^2$. A similar situation is encountered for VS cells, where the area of confidence again ranges from 50 to 100 Ωcm along the R_i axis and from 1 to 2 $\text{k}\Omega\text{cm}^2$ along the R_m axis. Of course, none of these ranges along one axis can be considered independently from the other axis, and certain interpolation techniques or more fine-scale parameter searches would yield more precise values in this respect. However, the main purpose of this investigation was to roughly estimate the area of confidence for the passive membrane parameters given the available experimental data including the statistical fluctuations inherent in the measurements.

3.6. *Role of Membrane Capacitance*

How much does this error function vary with different values chosen for the specific membrane capacitance C_m? To answer this question, the error value for HS cells is shown in Fig. 8 as a function of R_m, R_i and C_m. As can be seen from the five stacked contour plots, the area of confidence elongated and shifted toward smaller values for the internal resistivity R_i when smaller values for the specific membrane capacitance C_m were assumed, while the optimum for the specific membrane resistance R_m remained constant at 2 $\text{k}\Omega\text{cm}^2$. However, when looking at the absolute values of the error function in this 3D space, the absolute maximum and hence the optimal fit was yielded for HS cells for a specific membrane capacitance C_m between 0.75 and 1.0 $\mu\text{F/cm}^2$.

3.7. *Variability Within Cell Families*

To examine the variability of the electrotonic properties between different members of each cell family (see Fig. 1) we calculated the amplitude and phase spectra for each cell individually, taking the optimal values for passive membrane parameters as derived above. The results are shown in Figs. 9(a) and (b) for one HSN, HSE, and HSS cell, respectively. There existed slight differences in the steady-state input resistance, which ranged from 4 to 5 MΩ. However, the overall impression is that the fine anatomical differences that exist between these members of the HS cell family did not have any major impact on their electrotonic properties. Similar results are obtained when comparing different VS cells or various reconstructions from identical cells stained in different animals (data not shown).

3.8. *Influence of Recording Site*

Another question pertains to the influence of the site of the electrode placement on the result of the simulations. How much did the exact placement of the recording electrode in the simulation affect the amplitude and phase spectra? To answer this question we varied the site of the electrode in the simulations in three steps of 100 microns along the axon of a digitized HSE cell (Fig. 9(c), inset). For each location we determined the amplitude and phase spectra taking the passive membrane parameters of HS cells as determined previously (Figs. 9(c) and (d)). As the simulated electrode was moved toward the axon terminal, the steady-state input resistance increased substantially. Thus, the site of electrode placement has a significant effect on the optimum membrane parameters found by the fitting procedure described above.

3.9. *Influence of Tissue Shrinkage*

A possible source of error is connected to the shrinkage of the tissue due in the histological treatment of the

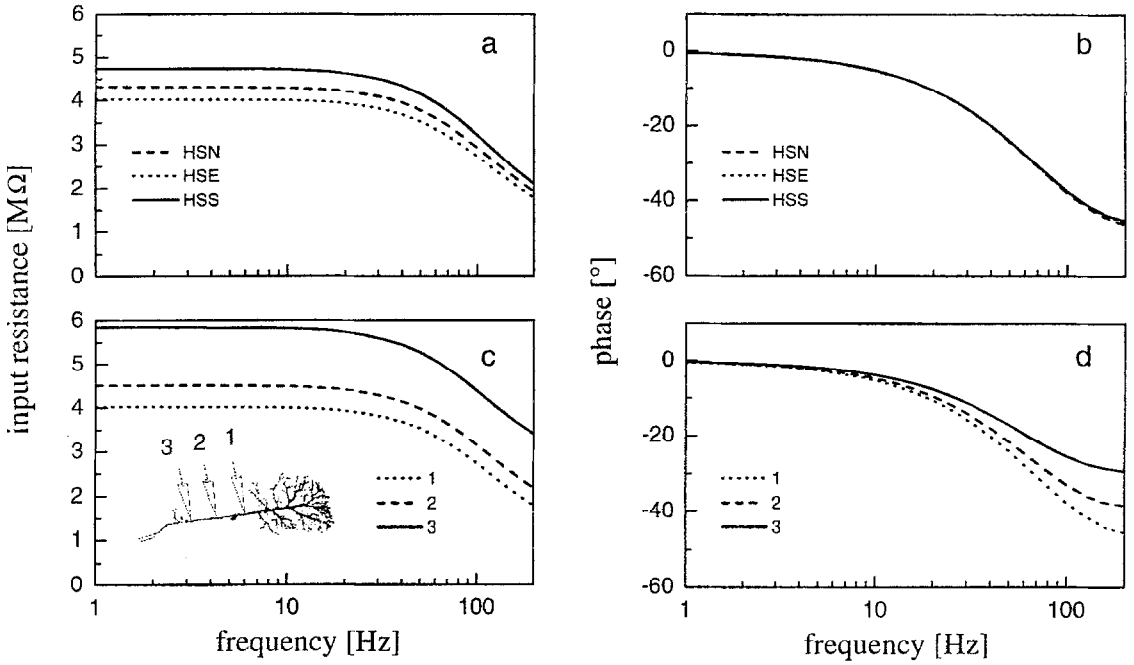

Figure 9. Amplitude (a) and phase spectra (b) of three different HS cells (HSN, HSE, and HSS cell, from top to bottom) as obtained from compartmental model simulations taking into account the detailed anatomy of each cell type. All three cells were modeled using the same passive membrane parameters. Note that, in general, the data are very similar for the different cells, and that variation mainly pertains to the steady state input resistance (between 4 and 5 MΩ). Amplitude (c) and phase spectra (d) for three different electrode placements in the same compartmental model neuron (HSE-cell). To the left the cell is shown with the recording electrode used for the simulations. As can be seen, as the electrode moves toward the axonal terminal, the steady-state input resistance increases and the high-frequency phase-shift becomes less pronounced. For details of the simulation procedure see legend of Fig. 6.

brain after filling the cells. Taking anatomical markers such as the diameter of the brain, we observed a shrinkage of about 15 to 20%, depending on the axis along which measurements were taken (see Material and Methods). However, we were not able to measure, within one and the same cell, how much this overall tissue shrinkage affects the exact diameter of the cells. To test how much shrinkage could, in principle, lead to erroneous membrane parameters, we compensated for shrinkage by inflating all cells of our data base isometrically by 20%. We then varied all membrane parameters in the way described above and determined those parameter triplets leading to the best fit with the experimental data. We found the following values (compare with Table 1): $R_m = 3.5$ kΩcm^2, $R_i = 80$ Ωcm, and $C_m = 1.2$ μF/cm^2 for CH cells with an error of 0.59; $R_m = 3.0$ kΩcm^2, $R_i = 40$ Ωcm, and $C_m = 0.6$ μF/cm^2 for HS cells with an error of 0.61; $R_m = 2.5$ kΩcm^2, $R_i = 60$ Ωcm, and $C_m = 0.7$ μF/cm^2 for VS cells with an error of 0.56.

3.10. Reliability of Results

How much can we rely on the findings provided by the parameter fitting to the amplitude and phase spectra? One critical experiment involved the injection of hyperpolarizing current pulses into the cells. In Fig. 10, left panel, the responses of CH, HS, and VS cells (solid lines, from top to bottom) to a current step of −2 nA amplitude are shown. The cells were hyperpolarized constantly by injection of a DC current of −4 nA to keep active membrane processes from contaminating the measurements. In this sample of CH cells, the steady-state input resistance was slightly larger than determined in the experiments shown in Fig. 5(b). For HS and VS cells, the respective values were almost identical to the ones determined previously. The middle and right panels display the time constants and their amplitudes derived from fitting a double exponential function to the step response of the cells. No error bars are shown in the plot, since fitting was done after the responses of the individual cells were averaged.

Table 2. Fly cell step response.

Cell family	τ_0 (ms)	τ_1 (ms)	A_0 (mV)	A_1 (mV)
CH cells	4.96	0.66	5.78	4.36
HS cells	2.10	0.63	6.85	2.99
VS cells	2.90	0.82	3.73	6.18

This was necessary since fitting exponential curves was rather noise sensitive and occasionally occurring epsps and other events contaminated the time course of individual response traces. As was verified in control runs, fitting a triple exponential function did not result in substantial changes in the first two time-constants and also did not improve the quality of the fit significantly (data not shown). Moreover, the fitting procedure was repeated several times with varying start values to make sure that the results did not represent local minima. The parameters of the double exponential fit can thus be regarded as a reliable description of the passive step responses of the cells studied here.

The results are summarized in Table 2. For all three cell types, the largest time constant was between 2 and 5 ms, and the second one was smaller than 1 ms. CH cells had the largest time constant of all three cell families considered here. Thus, HS and VS cells are rather fast and similar in this respect, while CH cells are significantly slower. This reflects the overall appearance of the pulse response and also agrees with the different cut-off frequencies as determined from the amplitude spectra (see Fig. 5(b)).

To compare these results with the response properties of the model cells, we repeated the same experiment with various compartmental model cells of each cell family. The passive membrane parameters used in the model simulations were the optimal values as derived from the fit to the amplitude and phase spectra. The model responses were obtained from averaging the responses of 2 CH cells, 6 HS cells, and 4 VS cells all taken from the data base. The time-courses fit the experimental results well (Fig. 10, left panels, dashed lines), except for CH cells, where the steady-state level assumed by the model cells is about 10% smaller than the measurements. Again, the resulting step responses were subjected to a double exponential fitting procedure, which was repeated several times with varying start values. The resulting time constants are shown as dashed bars in the middle and right panels of Fig. 10 and are summarized in Table 3. These data also indicate that CH cells differ from HS and VS cells significantly. First, the time constant τ_0 was longer for CH cells than for the other cells. Moreover, for CH cells,

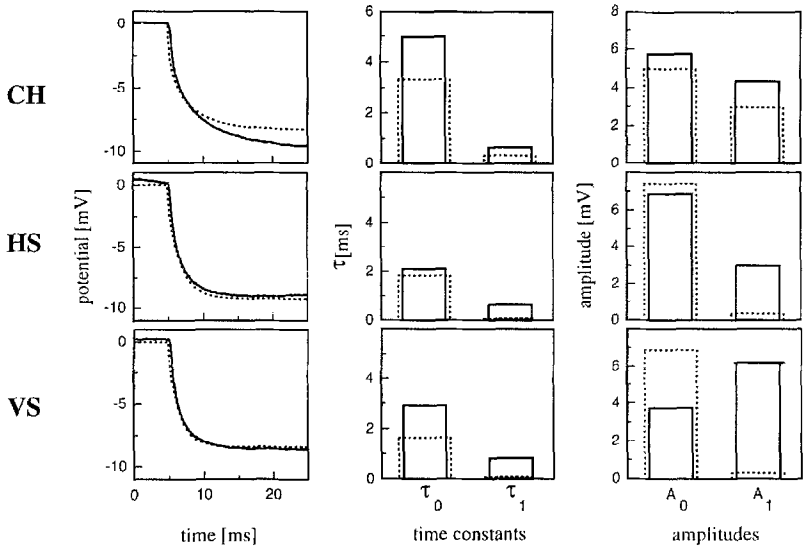

Figure 10. Responses of lobula plate tangential cells of the fly (solid lines) and of respective compartmental model cells (dashed lines) to injections of a hyperpolarizing current pulse of −2 nA (left panel). When a double exponential function of the form $f(t) = A_0 e^{-t/\tau_0} + A_1 e^{-t/\tau_1}$ is fitted to the response traces, the time constants τ_0 and τ_1 with the respective amplitudes A_0 and A_1 were determined, which are shown in the middle and right panel. Experimental data are shown as solid bars, model responses as dashed bars. Experimental data are averages obtained from 5 CH cells, 7 HS cells, and 6 VS cells. Model responses were obtained from 2 CH cells, 6 HS cells, and 4 VS cells of the data base. Cells were modeled as electrically passive units using the membrane parameters given in Fig. 6 and Table 1.

Table 3. Model cell step response.

Cell family	τ_0 (ms)	τ_1 (ms)	A_0 (mV)	A_1 (mV)
CH cells	3.33	0.33	4.98	2.97
HS cells	1.82	0.07	7.38	0.35
VS cells	1.64	0.07	6.87	0.30

the second time constant τ_1 contributed significantly to the response amplitude, whereas in the other two cell families the time constant τ_1 was negligible. Comparing these simulation results (Fig. 10, middle and right panels, dashed bars) with the experimental data shown in Fig. 10, the closest similarity was seen with respect to the first time constant τ_0. This pertains to all cell types considered here. However, the second time constant τ_1 was significantly longer in the experimental data than in the simulations. Moreover, the amplitude A_1 of the exponential function with this time constant was also larger in the data than in the simulation results. Thus, whereas with respect to the overall time course of the response to a step-like current injection experimental and simulated responses agree fairly well, substantial differences exist with respect to higher-order time constants and their contribution to the time course of the responses.

3.11. Electrotonic Models of Tangential Cells

The anatomy of the tangential cells, together with their passive membrane parameters as determined in this article, give rise to their electrotonic characteristics. This can be represented with the steady-state membrane potential distribution following a depolarizing current pulse of sufficient length at a single location in a false color code. Figure 11 shows the result of such a simulation for one member of each of the three cell families (CH, HS, and VS cells, from top to bottom). The result can be summarized as follows. In all three model cell types, a simulated current injected into the axon spread significantly to each side and lead to substantial voltage changes also in the main dendritic arborizations. In CH cell models, however, the potential dropped to almost 20% when measurements were taken in fine and distant branches of its dendrites. In contrast, in HS and VS cell models, the voltage dropped to only about 70 to 80% in the dendritic tips. It should be kept in mind, however, that values about voltage attenuation are in general not symmetrical (Zador et al., 1995). Considering dendritic current injection, voltage attenuation was much more pronounced than in the other direction. Here, only about 2% of the dendritic membrane potential reached the main axon of CH cells, and about 15 to 25% in HS and VS cells when current was injected into a single dendritic branchelet (Haag and Borst, 1997).

4. Discussion

Based on the 3D-reconstructed and digitized anatomy of the fly lobula plate tangential cells, we determined their passive membrane parameters by fitting the responses of compartmental models of the cells to experimentally determined amplitude and phase spectra, as obtained from injection of a sinusoidally modulated current of variable frequency into the axon of the cells. The results differed slightly for the different cell types under study. The exact parameters are summarized in Table 1. In the following section, the method of how these values were assessed will be critically discussed. Moreover, the values obtained for the fly visual interneurons will be compared to the ones published in the literature for other neurons.

4.1. Digital Data Base

All of the tangential cells have been described in extensive anatomical details before (Pierantoni, 1976; Hausen, 1982b; Hengstenberg et al., 1982; Eckert and Dvorak, 1983), but in a way that prevented the anatomical data from being used in computer simulations. The VS cells have even been 3D reconstructed, stored in digital form and displayed as stereo images (Hengstenberg and Hengstenberg, 1980), but the details and the format of the file structure does not allow these data to enter compartmental model software like Nemosys, Genesis, or Neuron (Eeckman et al., 1994; Hines, 1995; Bhalla et al., 1992). It was therefore necessary to redo the reconstruction of individual tangential cells using the set up as described in Material and Methods. As was tested by reconstructing an identical neuron twice by two different people, both the operation of the motorized stage as well as the precision of the operators was adequate yielding an error of below 5% in the anatomical data. All anatomical data, however, are affected to some extent by tissue shrinkage. We, nevertheless, did not compensate for tissue shrinkage because (1) the exact influence on the diameter of the

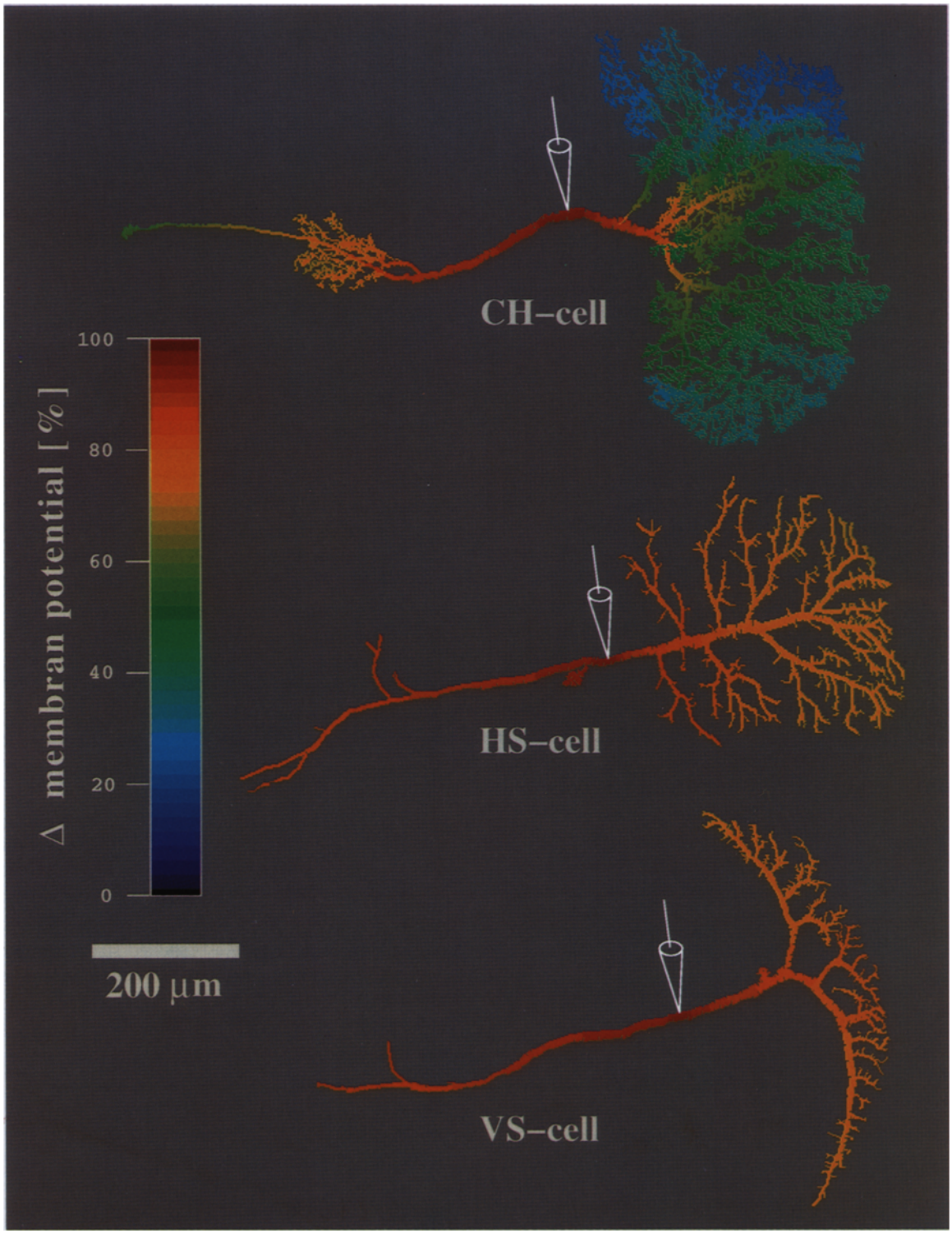

Figure 11. Simulated steady-state membrane potential distribution in CH, HS, and VS cells (from top to bottom) assuming only passive membrane properties (parameters given in Fig. 6 and Table 1). The simulation result is given in false color code assuming an injection of a DC depolarizing current of 10 nA into the axon of the cell. The color scale was chosen such as to cover the range between the resting state of the cell (dark blue) and the maximum depolarization reached at the injection site (red). Note that HS and VS cells are electrically more compact than CH cells.

process is not known, and (2) shrinkage does not exceed the variation in size of the cells when taken from different individuals.

4.2. *How to Determine Passive Membrane Parameters*

In principle, if we assume spatially homogeneous membrane parameters, and if the anatomy of a nerve cell is known precisely, there are three unknowns that have to be extracted from experimental measurements: the specific membrane resistance (R_m), the specific internal resistivity (R_i), and the specific membrane capacitance (C_m). To solve this problem, one needs three linearly independent equations—that is, three measurements where these three unknowns have different effects on the result. For a simple geometrical structure like a cylinder of length l and a constant diameter d, there exist exact recipes to do so (Rall, 1969). One can, for example, inject a step-like current into one end of the cable and measure (1) the steady-state input resistance at this location, (2) the steady-state voltage at a distance x with another electrode, and (3) the slowest time-constant inherent in the membrane response at the injection site. The following formulas relate the three variables to the measurements indicated above (see Rall, 1989; Traub and Miles, 1991, for further reading on these issues). The first formula gives the space constant λ, the distance over which a potential $V(0)$ drops to $1/e = 37\%$ of $V(0)$ in an infinitely long cable, as a function of R_m and R_i:

$$\lambda = \sqrt{d/4 * R_m/R_i}. \tag{6}$$

Defining L as the the physical length l of the cable divided by the space constant λ, the steady-state input resistance is determined by R_m and R_i in the following way:

$$\begin{aligned} R_{\mathrm{IN}} &= R_i * \frac{4}{d^2\pi} * \lambda * \coth(L) \\ &= \frac{2}{\pi} * \sqrt{1/d^3} * \sqrt{R_m R_i} * \coth(L). \end{aligned} \tag{7}$$

Since, $\lim_{L\to\infty} \coth(L) = 1$, the input resistance for semi-infinite cables becomes

$$R_{\mathrm{IN}} = \frac{2}{\pi} * \sqrt{1/d^3} * \sqrt{R_m R_i}. \tag{8}$$

Equation (7) links the first measurement to R_m and R_i. Next, the voltage drop over a distance x, determined in the second measurement, depends on R_m and R_i in the following way:

$$V(x) = V(0) * \frac{\cosh(L - x/\lambda)}{\cosh(L)}. \tag{9}$$

Finally, in the third measurement, the membrane time constant is linked to R_m and C_m in the following way:

$$\tau_m = R_m * C_m. \tag{10}$$

Having done these measurements, knowing the diameter d and length l of the nerve cell, and having a cell that can be either approximated directly as a cylinder or indirectly after collapsing the dendritic tree into one electrical equivalent cylinder, the critical parameters R_m, R_i, and C_m can be determined unambigously (Rall et al., 1992). However, there are some problems attached to this approach. The first problem exists with the determination of the slowest time constant of the response to a step like current. One way consists in the peeling process whereby in a semilogarithmic plot several time constants should be immediately visible (Rall, 1969). Another way of doing it consists in the fitting of several exponentials to the cellular response. However, reality is noisy. Therefore, time constants can appear in the fit with rather small amplitudes. There is no objective criterion based on which the significance of such small amplitude time constants can be determined. See Holmes et al. (1992) for an exhaustive discussion of this point. Another problem pertains to the often complicated anatomy of the cells where again it is unclear to what extent simplifications are allowed without leading to erroneous conclusions. In particular, for collapsing a branched structure into an equivalent cylinder, the daughter branches have to obey the '$d^{3/2}$-law' ($d^{3/2} = d_1^{3/2} + d_2^{3/2}$). Thus, a more practically oriented approach consists in doing a set of measurements (in principle, the more data, the better), digitizing the respective nerve cells, and then trying to explore the parameter space to see for which set of parameters an optimal fit between experiment and model can be obtained.

The question remains what kind of measurements should be done. The different possibilities have all in common that current should be injected in some dynamic way. Otherwise, when only steady-state conditions are being considered, there is no way of knowing the specific membrane capacitance C_m because this

parameter has no effect on the steady-state response of a nerve cell. Among the various possibilities of the waveform the injected current can have are white noise, a step function, a delta-pulse function, or a sinusoidal current of variable frequency. One advantage of using white noise is the speed by which the whole frequency range can be assessed in comparison with the explicit injection of each particular frequency when using the sinusoidal current. A second advantage is that assumptions of linearity can be tested with data sets derived from white noise analysis. We decided to use sinusoidal current injection at variable frequencies for our analysis and used the step-like current injection for later confirmation of the validity of the membrane parameter adjustment to the experimentally determined amplitude and phase spectra. A final decision of whether the experimental method was appropriate or not can be done only when considering the resulting error function in detail: only this inspection can tell how much the experiments restricted the volume space subtended by the error as a function of R_m, R_i, and C_m (see below).

4.3. *Relevance of Error Function*

The definition of the error function used to fit the passive parameters in this article is somewhat arbitrary but offers some generally advantageous properties. The first advantage lies in the applicability of this approach toward the analysis of a combination of different physical measures. In this study, amplitudes and phase angles were measured that have some obvious link in physics. In general, however, they could be completely different measures. How shall these entities be subsummed into a single value? The solution given here consists in scaling each individual error—the amplitude and the phase error—by the respective standard error of the mean. This has two advantages: (1) the resulting ratios are dimensionless and can, thus, be combined into a single error value, and (2) the error value as defined by its relation to the statistical fluctuations of the data turns into a quantitatively meaningful entity. The scaling procedure puts equal weight on each of the measurements, having the nice side effect that if the summed ratios (divided by 2) are equal to 1, the error in the simulated data exactly equals the noise inherent in the experimental measurements. This error can thus be used to outline an area (or volume) of confidence within which the parameter pairs (or triplets) are still compatible with the available data. Since the scaling factor equals the standard error of the mean, it is to be expected that the real membrane parameters fall within this region with a probability of 68%. Taking the negative logarithm of the error for the purpose of display just turns this criterion to be zero and expands the representation of the values within the area of confidence where the original error values are smaller than one.

Instead of combining two sorts of measurements into one error signal, one could also have considered using each set of experiments separately, pulled out the optimal fit values and compared them. But then the question would arise of how to combine the results of two such measurements. Should they be averaged? If not, the error functions could be combined in an appropriate way, and the peak be determined afterwards. But, again, how should the error functions be combined? If they are interpreted as probability functions, one immediately thinks about forming their product, but this would correspond to an assumption of statistical independence of the two measures, which they clearly are not. Since all these issues are theoretically still unclear, the way we combined both measurements into one error signal seems to make the least assumptions and, hence, is the most straightforward solution to the problem.

4.4. *Test of Reliability*

Whether the exact formula used in the calculation of the error signal is of decisive importance for the resulting membrane parameters has been examined by varying the error function in several ways (data not shown). We first used the logarithm of the amplitude spectra before calculating the differences between experimental and simulation data. We also boosted the weight of the low-frequency data points in order to compensate for the fact that when viewed on a logarithmic scale, the data points seem to be rather sparse in this frequency range (we explicitly decided to do only few measurements in the low frequency range because the input resistance does not change much here as compared to the region above the cut-off frequency). None of these manipulations altered the optimal fit found by the error function and only slightly altered the error function. Thus, the precise definition of the error function does not seem to have a critical effect on the resulting fit parameters.

Some skepticism on the validity of the results might arise from the comparison of the compartmental model responses with actual experiments in which current was injected using a step waveform. The step response

showing the most pronounced difference from the models is the one of the CH cells. Here, the steady-state value assumed after 50 ms differs between model and experiment. The reason for this difference lies in the fact the average steady-state input resistance of the cells in this sample is somewhat larger than in the sample that was used for measurements of the amplitude and phase spectra.

For the other cell types, the time course of the measured-step responses coincides well with the model responses. However, even in these cases, larger differences become visible when looking at the parameters of the double exponential analysis of the time courses. The fit between model and measured values only holds for the slowest time constant where deviation is in the range of about 30 to 50%. This is the most critical value, since it represents the membrane time constant. The smaller time constant, however, differs by almost an order of magnitude in case of HS and VS cells. This so-called equalization time constant arises from redistributing currents along the cable of the nerve cell.

Does this difference merely reflect the sensitivity of fitting double exponential functions to the response curves, or would we arrive at completely different sets of membrane parameters when using the step-responses as our fitting criterion? As one can readily see in the left panel of Fig. 7, model and cell responses coincide extremely well for HS and VS cells. Thus, despite the fact that the exponential fit led to pronounced differences with respect to the fast time constant, the overall appearance of the time courses of the responses including the steady-state value is similar. We therefore conclude that the parameter fit using the amplitude and phase spectra lead to a good estimate of the passive membrane parameters. Extracting time constants from a step response seems somewhat sensitive to experimental noise. Therefore, such higher-order features of the response are unlikely to yield reliable results.

4.5. *Comparative Aspects*

The membrane parameters determined in this article for the lobula plate tangential cells of the fly can be compared with values published for other cell types and other species in the literature. The preparations listed in Table 4 comprise the giant axon of the squid *Loligo*, various insect species, and pyramidal cells of the mammalian cortex or hippocampus. The way the authors arrived at these values differed from study to study. In some cases, the authors could penetrate the nerve cell at several locations simultaneously measuring time constants and length constants directly (see above). In most cases, however, the cells studied were too small to allow for such measurements. Here, a strategy similar to the one used by us was applied. If no satisfying fit between experimental and simulated data could be obtained, the assumption of homogeneous membrane parameters had to be dropped, and the cell was split into various regions. An example of such a case is given in the work of Shelton (1985) on Purkinje cells and in van Hateren and Laughlin (1990) on fly lamina monopolar cells.

All in all, each of the papers cited has to be scrutinized individually to get an idea about the validity of the membrane parameters stated in the respective paper. The value for the specific membrane resistance R_m varies the most (for nearly 3 orders of magnitude) and ranges from about 300 Ωcm^2 for the giant axon of the cockroach (Pichon, 1974) to 170,000 Ωcm^2 for the photoreceptor axon of the barnacle (Shaw, 1972) or hippocampal pyramidal neurons (Albowitz and Kuhnt, 1993). In contrast, the specific internal resistivity R_i ranges only over one order of magnitude between 30 (squid giant axon, Cole and Hodgkin, 1939) and 300 Ωcm (CA3 hippocampal pyramidal neuron, Jonas et al., 1993) or 380 Ωcm (cortical pyramidal neuron, Stratford et al., 1989). The value differing the least is the specific membrane capacitance C_m. This, however, needs to be qualified, since only few studies allowed for variation of the specific membrane capacitance. The values as determined for the fly tangential cells seem to be within the range of the literature values. However, for both R_i and R_m values, they are located toward the lower end of the range of data published.

4.6. *Spatial Homogenity of Membrane Parameters*

A critical point not discussed so far is the assumption of spatial homogenity of the membrane parameters. Of course, as soon as this assumption is being dropped, an almost infinite number of parameter constellations will be found that lead to a close fit between compartmental model behavior and real fly cells. However, in contrast to the passive membrane properties of Purkinje cells or fly lamina monopolar cells (Shelton, 1985; van Hateren and Laughlin, 1990) there is no need to assume spatially inhomogeneous membrane parameters in lobula plate tangential cells of the fly. This could be due to the fact that in this study, current injection was confined to the major process of the cells. Future

Table 4. Passive membrane properties of different cell types.

Cell type	R_m ($\Omega \cdot cm^2$)	R_i ($\Omega \cdot cm$)	C_m ($\mu F/cm^2$)	Source	Evidence
Squid giant axon	700	30	1.0	(Cole and Hodgkin, 1939)	Experiment
Barnacle photoreceptor	Axon: 170,000 Soma: 520	270 —	1.2 —	(Shaw, 1972)	Experiment
Crayfish medial giant neuron	2,000	60	1.6	(Glantz and Viancour, 1983)	Experiment
	870 (circum-oesophagal)	97	—		Experiment
	1,600 (abdominal)	100	—	(Yamagishi and Grundfest, 1977)	Experiment
	2,109	—	—	(Yamagishi and Grundfest, 1977)	Experiment
Crayfish lateral giant neuron	2,530	90	0.6	(Watanabe and Grundfest, 1961)	Experiment
Crayfish mechanosensory axon	2,617	160	3.5	(Mellon and Kaars, 1974)	Experiment
Crayfish lamina monopolar cell	2 400	60	—	(Wang-Bennett and Glantz, 1987)	Experiment
Lobster motor neuron	2,290	61	1.3	(Hodgkin and Rushton, 1946)	Experiment
Lobster medial giant neuron	2,434	95	0.8	(Tobias, 1960)	Experiment
Crab axon	7700	90	1.1	(Hodgkin, 1947)	Experiment
Fly lamina monopolar cell axon	>50,000	80	1.0	(van Hateren and Laughlin, 1990)	Experiment
Cockroach giant axon	293–942	46	3.3–6.3	(Pichon, 1974)	Experiment
Cockroach motoneuron	20,000–50,000	130	1.0	(Hochner and Spira, 1987)	Experiment
Cat alpha motoneuron	2,500	70	2.0	(Barrett and Crill, 1974)	Experiment
Spinal motoneuron	6,000	100	1.0	(Dodge and Cooley, 1973)	Simulation
Mouse dorsal root ganglion cell (culture)	7,000	—	1.0	(Brown et al., 1981b)	Experiment
Hippocampus CA1 pyramidal cell	Patch: 28,000	—		(Spruston and Johnston, 1992)	Experiment
	Intra: >5,000	—	2.0	(Traub and Llinas, 1979)	Experiment
	Intra: 15,000	—	—	(Brown et al., 1981a)	Experiment
	Intra: 85,100	199	0.7	(Major et al., 1993)	Experiment
Hippocampus CA3 pyramidal cell	Patch: 43,000	—	1.0	(Spruston and Johnston, 1992)	Experiment
	Patch: 164,000	294	0.683	(Jonas et al., 1993)	Experiment
	Intra: >10,000	—	2.0	(Traub and Llinas, 1979)	Experiment
	Intra: 19,000	—	—	(Brown et al., 1981a)	Experiment
Hippocampus dentate granula cell	Patch: 43,000	—	1.0	(Spruston and Johnston, 1992)	Experiment
	Intra: 12,000	—	—	(Brown et al., 1981a)	Experiment
Mouse neuroblastoma cell (culture)	10,000	70	2.0	(Moore et al., 1988)	Experiment
Rat cortical pyramidal cell	12,000–160,000	286–378	0.9–1.1	(Stratford et al., 1989)	Experiment
Guinea pig purkinje cell	6,000	100	1	(Llinas and Pellionisz, 1977)	Simulation
	Dendrite: 45,740	225	1.16	(Shelton, 1985)	Simulation
	Soma: 760	225	1.16	(Shelton, 1985)	Simulation
	Dendrite: ≈100,000 Soma: ≈500	250	1.5–2.0	(Rapp et al., 1994)	Experiment

studies will explore whether the fine dendritic branches posses different electrical properties than the rest of the cell or whether, indeed, the fly lobula plate tangential cells can be well described by a single set of passive membrane parameters homogeneously distributed all over the cell. Since electrophysiological recordings are restricted to cellular processes that are at least a few microns in diameter, such investigations will require the application of new methods like optical imaging of membrane potential distribution in single cells using voltage-sensitive dyes (Ross and Krauthamer, 1984; Staub et al., 1994; Borst, 1995).

4.7. Functional Considerations

Given that the values of the membrane parameters of the lobula plate tangential cells as determined herein are correct, the data suggest a significant difference between CH cells on the one hand and HS and VS cells on the other hand, with respect to their electrotonic structure. Considering dendritic current injection in CH cells, only about 2% of the dendritic membrane potential will reach the axon of these cells while the percentage is about 10 times larger in HS and VS cells. From a functional point of view, HS and VS cells are, thus, much better adapted for an effective transmission of graded signals than CH cells. In this context, however, two recent anatomical findings are of importance: (1) while HS and VS cells are purely postsynaptic in their lobula plate arborarization (Hausen et al., 1980), CH cells possess input as well as output synapses in their large dendritic tree (Gauck et al., 1994); (2) in contrast to HS and VS cells, the protocerebral ramifications of CH cells are purely postsynaptic (Gauck, Egelhaaf, and Borst, in preparation). Thus, the signal flow is from the dendrite through the axon toward the protocerebrum in HS and VS cells, while in CH cells it is from the protocerebrum and the dendrite into the dendrite. In particular, dendritic input signals in CH cells just have to travel a few microns before reaching a presynaptic transmitter release site. Taken all these facts together, signal propagation in CH cells is completely different from HS and VS cells, and this fact is reflected in their electrotonic structure, too. It should, however, be kept in mind that passive membrane properties only form the physical basis for signal propagation in nerve cells. Active membrane processes may substantially alter and shape the response as recorded in the axon of these cells, in particular when non-steady-state conditions are being considered (Haag and Borst, 1996). These issues will be treated in more detail in two forthcoming papers on the active membrane properties and visual response characteristics of the lobula plate tangential cells of the fly (Haag et al., 1997; Haag and Borst, 1997).

Acknowledgment

We are grateful to J.P. Miller and F. Theunissen for developing the Nemosys software and for introducing their reconstruction technique to us. We thank M. Bauch and B. Bochenek for reconstructing the tangential cells, T. Brotz, V. Gauck, and S. Single for carefully reading the manuscript, J. Gould and T. Vetter for help with GL programming, and the referees for helpful comments on the manuscript.

References

Albowitz B, Kuhnt U (1993) Spread of epileptiform potentials in the neocortical slice: Recordings with voltage-sensitive dyes. *Brain Res.* 631:329–333.

Barrett JN, Crill WE (1974) Specific membrane properties of cat motoneurones. *J. Physiol.* 239:301–324.

Bhalla US, Bilitch DH, Bower JM (1992) Rallpacks: A set of benchmarks for neuronal simulators. *Trends Neurosci.* 15:453–458.

Borst A (1990) How do flies land? From behavior to neuronal circuits. *BioScience* 40:292–299.

Borst A (1991) Fly visual interneurons responsive to image expansion. *Zool. Jb. Physiol.* 95:305–313.

Borst A (1995) Periodic current injection (PCI): A new method to image steady-state membrane potential of single neurons *in situ* using extracellular voltage-sensitive dyes. *Z. Naturforsch.* 50c:435–438.

Borst A, Bahde S (1988) Visual information processing in the fly's landing system. *J. Comp. Physiol. A* 163:167–173.

Borst A, Egelhaaf M (1989) Principles of visual motion detection. *Trends Neurosci.* 12:297–306.

Borst A, Egelhaaf M (1990) Direction selectivity of fly motion-sensitive neurons is computed in a two-stage process. *Proc. Natl. Acad. Sci.* (USA) 87:9363–9367.

Borst A, Egelhaaf M (1992) In vivo imaging of calcium accumulation in fly interneurons as elicited by visual motion stimulation. *Proc. Natl. Acad. Sci.* (USA) 89:4139–4143.

Borst A, Egelhaaf M (1994) Dendritic processing of synaptic information by sensory interneurons. *Trends Neurosci.* 17:257–263.

Borst A, Egelhaaf M, Haag J (1995) Mechanisms of dendritic integration underlying gain control in fly motion-sensitive interneurons. *J. Computat. Neurosci.* 2:5–18.

Brotz TM, Egelhaaf M, Borst A (1995) A preparation of the blowfly (*Calliphora erythrocephala*) brain for in vitro electrophysiological and pharmacological studies. *J. Neurosci. Meth.* 57:37–46.

Brown TH, Fricke RA, Perkel DH (1981a) Passive electrical constants in three classes of hippocampal neurons. *J. Neurophysiol.* 46:812–827.

Brown TH, Perkel DH, Norris JC, Peacock JH (1981b) Electronic structure and specific membrane properties of mouse dorsal root ganglion neurons. *J. Neurophysiol.* 45:1–15.

Cole KS, Hodgkin AL (1939) Membrane and protoplasm resistance in the squid giant axon. *J. Gen. Physiol.* 22:671–687.

Dodge FA, Cooley JW (1973) Action potential of the motorneuron. *IBM J. Res. Develop.* 17:219–229.

Eckert H (1982) The vertical-horizontal neuron (VH) in the lobula plate of the blowfly, *Phaenicia. J. Comp. Physiol.* 149:195–205

Eckert H, Dvorak DR (1983) The centrifugal horizontal cells in the lobula plate of the blowfly *Phaenicia sericata. J. Insect. Physiol.* 29:547–560.

Eeckman FH, Theunissen FE, Miller JP (1994) Nemosys: A system for realistic single neuron modeling. In: J Skrzypek, ed. Neural Network Simulation Environments. Kluwer, Boston. pp. 114–135.

Egelhaaf M, Borst A (1993) A look into the cockpit of the fly: Visual orientation, algorithms and identified neurons. *J. Neurosci.* 13:4563–4574.

Egelhaaf M, Borst A (1995) Calcium accumulation in visual interneurons of the fly: Stimulus dependence and relationship to membrane potential. *J. Neurophysiol.* 73:2540–2552.

Egelhaaf M, Borst A, Warzecha AK, Flecks S, Wildemann A (1993) Neural circuit tuning fly visual neurons to motion of small objects. II. Input organization of inhibitory circuit elements revealed by electrophysiological and optical recording techniques. *J. Neurophysiol.* 69:340–351.

Egelhaaf M, Haag J, Borst A (1994) Processing of synaptic information depends on the structure of the dendritic tree. *Neurorep.* 6:205–208.

Franceschini N, Kirschfeld K (1971) Les phénomènes de pseudopupille dans l'oeil composé de *Drosophila. Kybernetik* 9:159–182.

Gauck V, Egelhaaf M, Borst A (1994) Electronmicroscopical and electrophysiological analysis of synaptic interactions in the circuit mediating figure-ground discrimination in the blowfly *Calliphora.* In: N Elsner, H Breer, eds. Göttingen Neurobiology Report 1994, Thieme. p. 445.

Geiger G, Nässel DR (1981) Visual orientation behaviour of flies after selective laser beam ablation of interneurones. *Nature* 293:398–399.

Geiger G, Nässel DR (1982) Visual processing of moving single objects and wide-field patterns in flies: Behavioural analysis after laser-surgical removal of interneurons. *Biol. Cybern.* 44:141–149.

Glantz RM, Viancour T (1983) Integrative properties of crayfish medial giant neuron: Steady-state model. *J. Neurophysiol.* 50:1122–1142.

Haag J, Borst A (1996) Amplification of high-frequency synaptic inputs by active dendritic membrane processes. *Nature* 379:639–641.

Haag J, Theunissen FE, Borst A (1997) The intrinsic electrophysiological characteristics of fly lobula plate tangential cells. II. Active membrane properties. *J. Computat. Neurosci.* (in preparation).

Haag J, Borst A (1997) The intrinsic electrophysiological characteristics of fly lobula plate tangential cells. III. Visual response properties. *J. Computat. Neurosci.* (in preparation).

Haag J, Egelhaaf M, Borst A (1992) Dendritic integration of motion information in visual interneurons of the blowfly. *Neurosci. Lett.* 140:173–176.

Hausen K (1981) Monocular and binocular computation of motion in the lobula plate of the fly. *Verh. Dtsch. Zool. Ges.* 74:49–70.

Hausen K (1982a) Motion sensitive interneurons in the optomotor system of the fly. I. The horizontal cells: Structure and signals. *Biol. Cybern.* 45:143–156.

Hausen K (1982b) Motion sensitive interneurons in the optomotor system of the fly. II. The horizontal cells: Receptive field organization and response characteristics. *Biol. Cybern.* 46:67–79.

Hausen K (1984) The lobula-complex of the fly: Structure, function and significance in visual behaviour. In: MA Ali, ed. Photoreception and Vision in Invertebrates. Plenum Press, New York. pp. 523–559.

Hausen K, Wehrhahn C (1983) Microsurgical lesion of horizontal cells changes optomotor yaw response in the blowfly Calliphora erythocephala. *Proc. R. Soc. Lond. B* 219:211–216.

Hausen K, Wehrhahn C (1990) Neural circuits mediating visual flight control in flies. II. Separation of two control systems by microsurgical brain lesions. *J. Neurosci.* 10:351–360.

Hausen K, Wolburg-Buchholz K, Ribi WA (1980) The synaptic organization of visual interneurons in the lobula complex of flies. *Cell Tissue Res.* 208:371–387.

Heisenberg M, Wonneberger R, Wolf R (1978) Optomotor-blind (H31): A *Drosophila* mutant of the lobula plate giant neurons. *J. Comp. Physiol.* 124:287–296.

Hengstenberg R (1982) Common visual response properties of giant vertical cells in the lobula plate of the blowfly Calliphora. *J. Comp. Physiol. A* 149:179–193.

Hengstenberg R, Hausen K, Hengstenberg B (1982) The number and structure of giant vertical cells (VS) in the lobula plate of the blowfly Calliphora erytrocephala. *J. Comp. Physiol. A* 149:163–177.

Hengstenberg R, Hengstenberg B (1980) Intracellular staining of insect neurons with procion yellow. In: NJ Strausfeld, TA Miller, eds. Neuroanatomical Techniques. Springer Verlag, New York. pp. 308–323.

Hines M (1995) The neuron simulation program. In: J Skrzypek, ed. Neural Network Simulation Environments. Kluwer, Boston. pp. 147–163.

Hochner B, Spira ME (1987) Preservation of motoneuron electrotonic characteristics during postembryonic growth. *J. Neurosci.* 7:261–270.

Hodgkin AL (1947) The membrane resistance of a non-medullated nerve fibre. *J. Physiol.* 106:305–318.

Hodgkin AL, Rushton WAH (1946) The electrical constants of a crustacean nerve fibre. *Proc. R. Soc. Lond. B* 133:444–479.

Holmes WR, Segev I, Rall W (1992) Interpretation of time constant and electrotonic length estimates in multicylinder or branched neuronal structures. *J. Neurophysiol.* 68:1401–1420.

Jonas P, Major G, Sakmann B (1993) Quantal components of unitary EPSCs at the mossy fibre synapse on CA3 pyramidal cells of rat hippocampus. *J. Physiol.* 472:615–663.

Llinas R, Pellionisz A (1977) A computer model of the cerebellar purkinje cells. *Neuroscience* 2:37–48.

Major G, Evans JD, Jack JJB (1993) Solutions for transients in arbitrarily branching cables: I. Voltage recording with a somatic shunt. *Biophys. J.* 65:423–449.

Mellon D, Kaars C (1974) Role of regional cellular geometry in conduction of excitation along a sensory neuron. *J. Neurophysiol.* 37:1228–1238.

Moore LE, Yoshii K, Christensen BN (1988) Transfer impedances between different regions of branched excitable cells. *J. Neurophysiol.* 59:689–705.

Pichon Y (1974) Axonal conduction in insects. In: JE Treherne, ed. Insect Neurobiology. North-Holland, Amsterdam. pp. 73–117.

Pierantoni R (1976) A look into the cock-pit of the fly. *Cell Tissue Res.* 171:101–122.

Rall W (1969) Time constants and electrotonic length of membrane cylinders and neurons. *Biophys. J.* 9:1483–1508.

Rall W (1989) Cable theory for dendritic neurons. In: C Koch, I Segev, eds. Methods in Neuronal Modeling: From Synapses to Networks. MIT Press, Cambridge, MA. pp. 9–62.

Rall W, Burke RE, Holmes WR, Jack JJB, Redman SJ, Segev I (1992) Matching dendritic neuron models to experimental data. *Physiol. Rev.* 72:S159–S186.

Rapp M, Segev I, Yarom Y (1994) Physiology, morphology and detailed passive models of guinea-pig cerebellar Purkinje cells. *J. Physiol.* 474(1):101–118

Ross WN, Krauthamer V (1984) Optical measurements of potential changes in axons and processes of neurons of a barnacle ganglion. *J. Neurosci.* 4:659–672.

Shaw SR (1972) Decremental conduction of the visual signal in barnacle lateral eye. *J. Physiol.* 220:145–175.

Shelton DP (1985) Membrane resistivity estimated for the Purkinje neuron by means of a passive computer model. *Neuroscience* 14:111–131.

Spruston N, Johnston D (1992) Perforated patch-clamp analysis of the passive membrane properties of three classes of hippocampal neurons. *J. Neurophysiol.* 67:508–529.

Staub C, de Schutter E, Knöpfel T (1994) Voltage-imaging and simulation of effects of voltage- and agonist-activated conductances on soma-dendritic voltage coupling in cerebellar purkinje cells. *J. Computat. Neurosci.* 1:301–311.

Stratford K, Mason A, Larkman A, Major G, Jack J (1989) The modelling of pyramidal neurones in the visual cortex. In: R Durbin, C Miall, G Mitchison, eds. The Computing Neuron. Addison Wesley, Wokingham, UK. pp. 296–321.

Strausfeld NJ, Hausen K (1977) The resolution of neuronal assemblies after colbalt injection into neuropil. *Proc. R. Soc. Lond. B* 199:463–476.

Theunissen FE, Tromp J, Eeckman FH, Miller JP (1996) Nemosys 3.1. Available by ftp. Contact fet@phy.ucsf.edu.

Tobias JM (1960) Further studies on the nature of the excitable system in nerve. *J. Gen. Physiol.* 43(2):57–71.

Traub RD, Llinas R (1979) Hippocampal pyramidal cell: Significance of dendritic ionic conductances for neuronal function and epileptogenesis. *J. Neurophysiol* 42:476–496.

Traub RD, Miles R (1991) Neural Networks of the Hippocampus. Cambridge, Cambridge University Press.

van Hateren JH, Laughlin SB (1990) Membrane parameters, signal transmission, and the design of a graded potential neuron. *J. Comp. Physiol. A* 166:437–448.

Wang-Bennett LT, Glantz RM (1987) The functional organization of the crayfish lamina ganglionaris. I. Nonspiking monopolar cells. *J. Comp. Physiol. A* 161:131–145.

Watanabe A, Grundfest H (1961) Impulse propagation at the septal and commissural junctions of crayfish lateral giant axons. *J. Gen. Physiol.* 45(1):267–308.

Yamagishi S, Grundfest H (1977) Regional differences in K-channels of abdominal and circumesophageal segments of the crayfish medial giant axon. *J. Membrane Biol.* 31:65–79.

Zador AM, Agmon-Snir H, Segev I (1995) The morphoelectrotonic transform: A graphical approach to dendritic function. *J. Neurosci.* 15:1669–1682.